Volume 18, Number 2, 2025. pp. 207-224

Jordan Journal of Physics

ARTICLE

Dimensionality Impact on Two Rydberg-Dressed Atoms Confined in a Harmonic Trap

Leila Chia[a,b] and **Nabila Grar**[b]

[a] *Laboratory of Materials Physics, Radiation and Nanostructures, University Mohamed El Bachir El Ibrahimi of Bordj Bou Arreridj 34000, Algeria.*

[b] *Department of Material Sciences, University Mohamed El Bachir El Ibrahimi, Bordj Bou Arreridj 34000, Algeria.*

Doi: **https://doi.org/10.47011/18.2.10**

Received on: 18/12/2023; *Accepted on: 20/02/2024*

Abstract: An analytical solution is possible for the Schrödinger equation for two particles interacting via a step-like potential and confined in a harmonic trap. This model is assumed to be very close to the real case of two confined Rydberg-dressed atoms. In this contribution, we thoroughly examine the validity of this approximation to describe the realistic situation. We analyze in detail the impact of the dimensionality on the spatial correlation of the system. The impact of the dimensionality on the dynamics of the system under a quench scenario is also investigated.

Keywords: Two atoms in a harmonic trap, Cold Rydberg atoms, Analytical solution of the Schrödinger equation, Spatial correlations, Quenching.

PACS: 31.15.ac; 03.65.-w; 32.50.+d.

1. Introduction

Matter is a huge and intricate assembly of some “fundamental” constituents, within which the individuality of these elements often appears to be lost. Understanding how finite micro elements lead to the macroscopic structure is of paramount importance in both nuclear and condensed matter physics. It aims not only to the comprehension of the constituents’ structure but also to the elucidation of the correlations and the interplay among constituents. On the other hand, experiments involving confined cold few particles are nowadays very accessible and are becoming a matter of routine. In fact, a number of system parameters, such as the confinement potential and the particle-particle interaction features, can be controlled on demand [1, 2]. This way, it is possible to verify experimentally the validity of a number of quantum simplified models studied in the past and explore fundamental physics concepts. It is also true that more efforts are necessary in order to devise new “toy” models targeting a detailed comprehension of the features of the interaction at different levels of approximation as well as different dimensionalities (1D, 2D, and 3D). An exact solution for the Schrödinger equation established in the case of different and sometimes complicated potentials, can be found in the literature (see, for example, Refs. [3-7]). Most of these solutions are given for the case of a single particle system. The situation becomes quite complicated when considering the case of two particles as a first step on the path towards the description of cold, confined few-body systems [8-10]. The difficulty resides in the consideration of both confinement potential characteristics and a realistic interaction potential. The hard-core interaction is the most simplified interaction scheme, and in this case, it is possible to achieve a quasi-exact solution for the two-particle

Corresponding Author: Nabila Grar **Email**: nabila.grar@univ-bba.dz

system. A theoretical study encompassing the three dimensionalities and a delta-like interaction for a system of two particles was developed in the seminal work of Busch *et al*. [11, 12]. In that work, a quasi-exact solution is derived under the assumption of a contact interaction (an s-wave for bosons and a p-wave for fermions). In order to take into account a certain interaction range, a Gaussian-like potential can be considered, which also allows for a quasi-analytical solution [13, 14]. These interaction models, however, ignore the long-range nature of the interaction for dipolar atoms or the Rydberg-dressed interaction behaving like $1/r^6$ and which can be very important either fundamentally or experimentally [15, 16]. An analytical solution for this interaction is still to be found. Nevertheless, a simplification of this interaction as a step function was proposed by Kościk *et al*. [17]. This approach enables a quasi-exact solution in one and two dimensions and allows for a detailed investigation of the system's various features. These quasi-solvable models are of extreme importance for advances in cold confined few-particle systems. It can be considered as a set of models to be validated experimentally as well as an exact basis to construct the solution for few-body systems exploiting different strategies, such as variational, *ab initio*, or interacting configurations [8-10]. The aim of the present study is to conduct a comparative analysis of the quasi-exact solvable model of Kościk *et al*. in the three dimensionalities and highlight the most important players for the considered interaction. We are unavoidably concerned by the analysis of the spatial correlations, which provide essential insight into the system's internal structure. We focus on the effects of the dimensionality on the spatial distribution of the system. The study is first established in a static regime and then enlarged to a dynamical one. In the dynamical regime, we are interested in the influence of the dimensionality on the evolution of the correlation under different quench scenarios. However, before proceeding with the details of the study, we establish the validity of using a step-function potential as a substitute for the more realistic Rydberg interaction is appropriate. To this end, we apply perturbation theory to identify potential discrepancies between results obtained using the approximate step function and those derived from the original long-range potential. The paper is organized as follows: In the second section, we review the key theoretical framework and provide the essential formulas and energy spectra relevant to the subsequent analysis. The third section presents a perturbative treatment of the system under the step-function potential and illustrates the convergence of its results toward those of the realistic interaction model. The fourth section is devoted to analyzing the energy spectra associated with the relative motion in the two-particle system for various interaction ranges, emphasizing the role of dimensionality. In this section, we also examine the relative radial spatial correlation and investigate the interplay between the centrifugal barrier, interaction range, and interaction strength in one, two, and three dimensions. In the fifth section, we present a time-dependent analysis of the system, focusing on the effects of dimensionality and sudden parameter changes (quench scenarios) on the evolution of spatial correlations. The main findings are summarized in the concluding section.

2. Theoretical Background

The different models aim to establish an analytical solution for the following Schrödinger equation for a system of two identical spinless quantum particles, having a mass m and trapped in an external potential:

$$\left(\sum_{i=1}^{2} \frac{-\hbar^2}{2m} \nabla_i^2 + v_{ext} + v\right) \psi(\vec{r_1}, \vec{r_2}) = E\psi(\vec{r_1}, \vec{r_2}), \quad (1)$$

where v_{ext} is the confining potential, v is the interaction potential depending on the particles' separation, and $\vec{r_i}$ is the vector position for each particle. To simplify the calculation, the particles are assumed to be point-like (structureless), and the confining potential is taken to be harmonic. The constraints imposed on the harmonic potential in different spatial directions determine the motion of the particles and thus define the dimensionality of the problem [18-20]. The same confining potential is imposed on both particles, and the equation becomes:

$$\left(\left(\sum_{i=1}^{2} \frac{-\hbar^2}{2m} \nabla_i^2 + \frac{1}{2} m\omega^2 r_i^2\right) + v(|\vec{r_1} - \vec{r_2}|)\right) \psi(\vec{r_1}, \vec{r_2}) = E\psi(\vec{r_1}, \vec{r_2}). \quad (2)$$

For this quadratic potential, it is possible to single out the center-of-mass contribution to the motion from the relative one. The equation then

becomes:

$$\left(\frac{-\hbar^2}{2M}\nabla_{\vec{R}}^2+\frac{1}{2}M\omega^2R^2+\frac{-\hbar^2}{2\mu}\nabla_{\vec{r}}^2+\frac{1}{2}\mu\omega^2r^2+v(r)\right)\psi(\vec{R},\vec{r})=E\psi(\vec{R},\vec{r}), \quad (3)$$

where $M=2m$, $\mu=m/2$ (the reduced mass), $R=|\overrightarrow{r_1}+\overrightarrow{r_2}|/2$, and $r=|\overrightarrow{r_1}-\overrightarrow{r_2}|$. The wave function can be written in a separable form as:

$$\psi(\vec{R},\vec{r})=\chi(\vec{R})\varphi(\vec{r}). \quad (4)$$

Consequently, we can separate the center-of-mass motion from the relative one as:

$$\left(\frac{-\hbar^2}{2M}\nabla_{\vec{R}}^2+\frac{1}{2}M\omega^2R^2-E_c\right)\chi(\vec{R})=0, \quad (5)$$

$$\left(\frac{-\hbar^2}{2\mu}\nabla_{\vec{r}}^2+\frac{1}{2}\mu\omega^2r^2+v(r)-E_r\right)\varphi(\vec{r})=0, \quad (6)$$

with $E=E_c+E_r$. The first equation is just an equation for a harmonic oscillator with known solutions. The difficulty resides in finding a solution for the second equation, where handling a realistic interaction can be quite challenging. It is important to note that the symmetry of the total wave function depends only on the relative part of the wave function since the center-of-mass part is symmetric by construction. Operating the adequate changes in the appropriate coordinate system [21], we can express Eq. (6) for three dimensions (1D, 2D, and 3D), respectively, as:

$$\left(\frac{-d^2}{dr^2}+\frac{1}{4}r^2+v(r)-E_r\right)f(r)=0, \quad (7)$$

$$\left(\frac{-d^2}{dr^2}+\frac{l^2-1/4}{r^2}+\frac{1}{4}r^2+v(r)-E_r\right)f(r)=0, \quad (8)$$

$$\left(\frac{-d^2}{dr^2}+\frac{l(l+1)}{r^2}+\frac{1}{4}r^2+v(r)-E_r\right)f(r)=0. \quad (9)$$

Here, the energy, the position, and the angular momentum quantum number l are expressed in $\hbar\omega$, $\sqrt{\frac{\hbar}{m\omega}}$, and $\sqrt{\hbar m\omega}$ units, respectively. The second term in Eqs. (8) and (9) represents the centrifugal potential. The last two equations are just the relative-radial part of the Schrödinger equation. Notice that we can shift from Eq. (8) to Eq. (9) by operating the following change:

$$l_{2D}\rightarrow l_{3D}+1/2. \quad (10)$$

This means that it is possible to find the solution for the 3D case by solving the equation for the 2D case, provided that the appropriate relation between the angular momentum quantum numbers is respected [17]. It is clear from the equations that the centrifugal effect is completely absent in 1D (Eq. 7) and is increasing when passing from 2D to 3D [Eqs. (8) and (9)]. It is also important to recall that the total wave function is defined by the quantum number n in 1D, by n and l in 2D, and by $n, l,$ and m in 3D. This wave function is symmetric for even n in 1D and even l for 2D and 3D; it is antisymmetric for odd n in 1D and odd l for 2D and 3D. A symmetric total wave function defines a bosonic state, whereas an antisymmetric total wave function defines a fermionic one.

Solving Eqs. (7), (8), and (9) relies on the form considered for the interaction potential. For our study, we are interested in the long-range nature of the interaction. This is the case for the interaction between two non-symmetric neutral charged distributions. Such interactions involve multipolar excitations, particularly when atoms are excited to high principal quantum numbers, known as Rydberg states [22]. The potential for this interaction can be approximated to the first order as composed of a short-ranged part, to which we add a van der Waals long-ranged interaction. This last one is the main contribution to the multipolar excitations. In this case, the interaction potential can be given as [17, 23]:

$$v(r)=\frac{g}{1+\left(\frac{r}{R_C}\right)^6}, \quad (11)$$

where g is the strength and R_c is the range of the potential (see Fig. 1). We will call this potential the Rydberg interaction in the following sections. It is not yet possible to find an exact solution to the Eqs. (7), (8), and (9) with this realistic interaction along with the harmonic confinement. Nevertheless, a quasi-exact solution is achieved for an interaction potential defined as a step function [17]. This approximation mimics the previous expression quite fairly for the short-range part and then falls abruptly to zero. It is given as:

$$v(x)=\begin{cases}v_0 \ pour\ x\leq a\\ 0\ x>a,\end{cases} \quad (12)$$

where we can relate v_0 and a to the strength and the range (g and R_C), respectively (Fig. 1) [17].

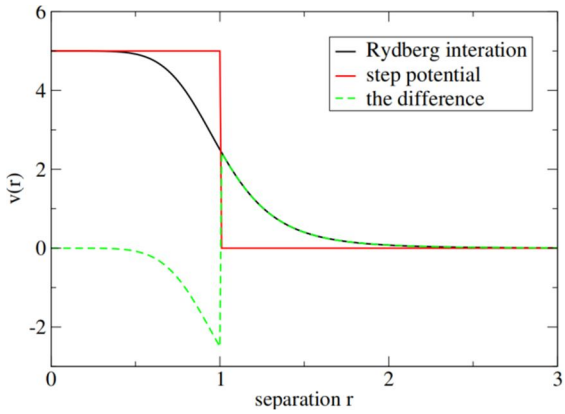

FIG. 1. Comparison between the realistic Rydberg interaction, the step function, and the difference between these two potentials. v_0 is set to 5, and the range is equal to one. The difference is considered as a perturbation (see Sec. 3).

This simplification is justified by the fact that the main contribution to the realistic potential comes from the flat part. In the case of this approximation, it is possible to establish a quasi-exact solution by reducing the 1D equation [Eq. (7)] to a Weber form, while the 2D and 3D relative-radial equations [Eqs. (8) and (9)] are transformed into Kummer-type differential equations. The solution is expressed as a function of the confluent hypergeometric function of the first kind in the region $[0, a]$, and as a function of the Tricomi function elsewhere [17, 24-26]. In order to guarantee a physical behavior of the whole solution, a condition for the continuity of the two functions and their derivatives is imposed at $r = a$, leading to transcendental equations. Solving these equations quantizes the energy, which allows for the retrieval of the energy spectrum with different combinations of strength v_0 and range a. Figs. 2 and 3 display representative energy spectra obtained from this model. Fig. 2 shows the energy versus the interaction strength for different values of the range in the case of 1D, whereas Fig. 3 is the same illustration for the 2D and 3D cases. These figures are mostly the same as the ones illustrated in [17, 27] and are reproduced here just to clarify and justify some of the results developed in subsequent sections. It is worth signaling the fermionization limits in 1D calculations where the bosons' energy levels are converging to the fermions' ones. This is known as the bosons-fermions mapping or the Tonks-Girardeau limit [28]. The results for the 3D case are similar to the 2D case but are shifted to higher energy levels. This result derives straightforwardly from the relation given by Eq. (10). This remark will be used to expect or justify some of the following results.

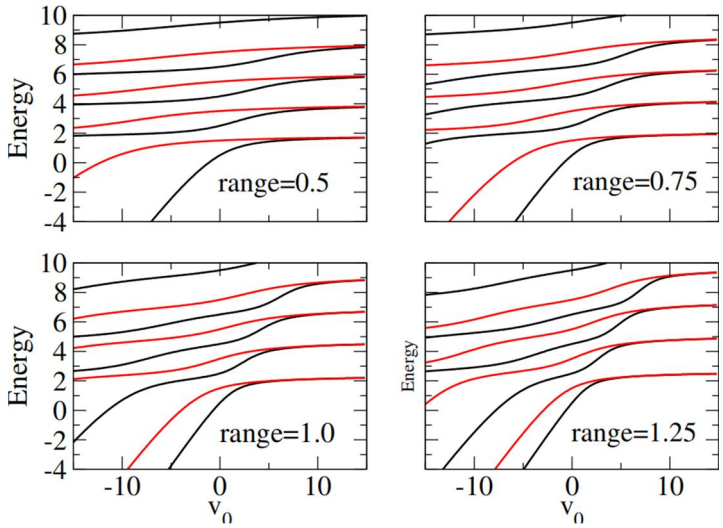

FIG. 2. (a) Energy spectrum in one dimension versus v_0 with increasing values of n (n = 0, 1 ... 8, bottom to top). Even values of n correspond to bosons (black), while odd values represent fermions (red). The value of the range a is indicated in each panel.

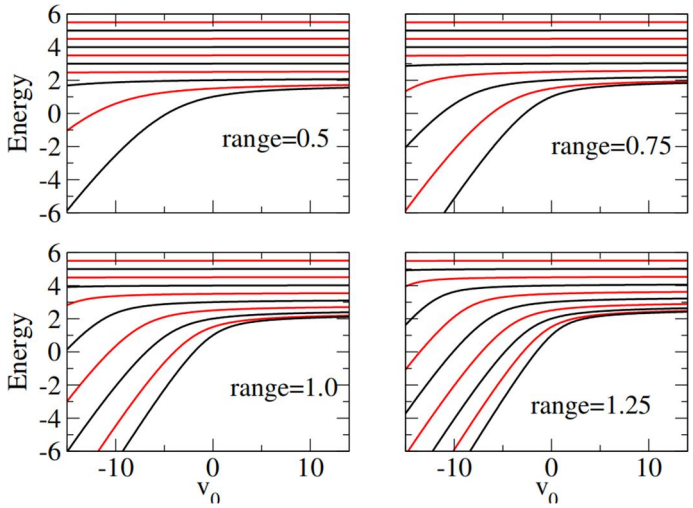

FIG. 3. Energy spectrum for the fundamental state (n = 0) versus v_0 with increasing values of the angular momentum quantum number $l = 0, 1, 2, 3, 4$ (from bottom to top) in three (red) and two (black) dimensions. The value of the range a is indicated in each panel.

These results are only possible for a harmonic trap and a step-like potential interaction, where an analytical solution is possible. Plenty of other complicated trap shapes, along with different interactions, are possible. However, only numerical approaches in these cases are used to investigate the system of two trapped particles [29].

3. Perturbation Treatment

Before proceeding to the main topic of this contribution, namely, the study of the impact of the dimensionality on some properties of the studied system, we first aim to assess the accuracy of approximating the Rydberg interaction with a step-function potential. We are interested in discrepancies between these two results by employing adequate tools in order to ameliorate the initial model. To this end, we employ perturbation theory to compare the following:

1. The analytical results for a step-like potential;
2. The numerical results for the exact formulation of the potential [Eq.(11)];
3. The results of the perturbation treatment of a step-like potential.

We have to clarify here that in the reference [17], both the numerical (Rydberg interaction) and analytical (step potential) results for the energy spectra are plotted on the same graphs, showing a discrepancy between these two results, a discrepancy that becomes more apparent for important ranges and in two dimensions. Similarly, in Ref. [30], an approximate value of the threshold interaction strength is calculated analytically for the step potential and compared to the numerical results for the Rydberg interaction. This is done in one dimension, and a tiny discrepancy is found between the two results. In our calculation, we are not only concerned with reporting the existing discrepancy but also try to bridge the gap between the two situations (numerical solution for the exact potential and the analytical solution for the step-like potential) for the cases of 3D, 2D, and 1D, using the perturbation tool. This calculation is important from two perspectives. First, reaching an agreement between the two results would confirm the adequacy of the step function as a replacement of the realistic Rydberg potential, as it confirms that the missing part is just a perturbation. Second, it would enable the construction of a more accurate wave function basis if a description of few-particle systems is targeted.

To start with, the exact potential is written as:

$$v(r) = \frac{g}{1+\left(\frac{r}{R_c}\right)^6} = v_s(r) - v_s(r) + \frac{g}{1+\left(\frac{r}{R_c}\right)^6} = v_s(r) + v_{pert}, \quad (13)$$

where $v_{pert}(r) = \frac{g}{1+\left(\frac{r}{R_c}\right)^6} - v_s(r)$ and $v_s(r)$ is the step function defined in Eq. (12). This way, it is possible to write the exact potential as a step function for which we already know the solutions and an extra quantity v_{pert} that we assume to be a perturbation. A plot for this potential for the case where the step is equal to 5 and the range of the potential is equal to 1, is illustrated in Fig. 1. The Numerov approach [31] is used to obtain the numerical results for the

exact potential (the Rydberg potential). In our case, the goal is to demonstrate that the perturbative approach applied to the step potential can reproduce the numerical results with high fidelity, thereby validating the approximation and enhancing our model's predictive power. Let us mention that we use a forward and inward integration method, and we impose the continuity of the wave function and its derivative at the turning points [31] to ensure the stability of the Numerov calculation. The perturbation correction is assumed to be of the first order for the eigenvalues and the eigenvectors.

3.1 Eigenvalues

The comparison of the eigenvalues (energies) versus v_0 for one dimension and different ranges is presented in Fig. 4. It is clear from this figure that the correction to the first order is sufficient to reach a fair agreement with the numerical results. Higher energy levels are less affected by the interaction according to their range, and are thus already too close to the numerical results. Conversely, the low levels are more affected by the interaction, making the correction for these levels quite important. This correction demonstrates an energy level for fermionization, which is higher than the one without the correction. In the same manner as previously, we extend the perturbation calculation to the radial part of the Schrödinger equation for 2D [Eq. (8)]. The perturbation potential is the same as before. The only difference is the centrifugal term making a logarithmic mapping and a transformation of the radial solution necessary for the densification of the points around zero for the wave function and for recovering the Numerov shape of the equation, respectively [31]. The comparison of the spectra versus v_0 and for different ranges a is illustrated in Fig. 5. The correction to the first order for both intermediate and large ranges is making the agreement with the numerical solution more satisfactory, especially for the repulsive regime (v_0 positive), where the curves are indistinguishable. In the attractive regime (v_0 negative), the corrected results for the lower levels are more satisfactory. The results for the 3D are quite similar to those of 2D (not shown here for brevity), as the only difference between the two cases is an addition in orbital momentum quantum number, which shifts the entire energy spectrum to higher values.

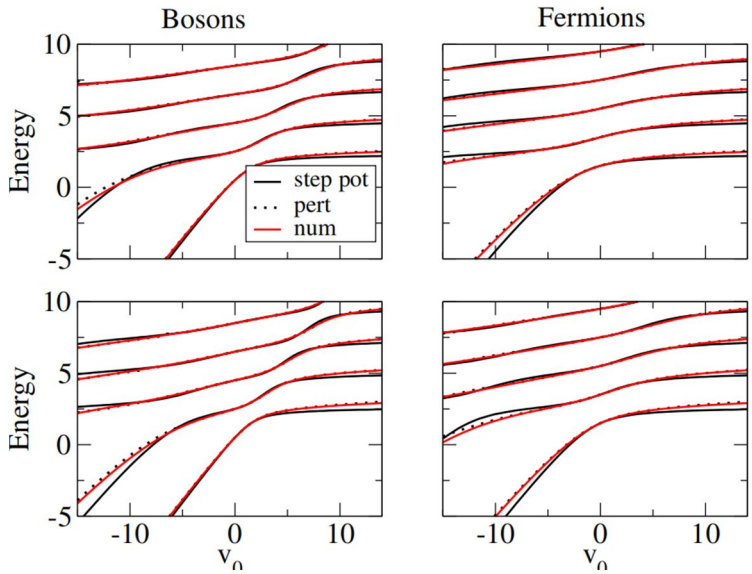

FIG. 4. Comparison of the energy versus v_0 for bosons and fermions (columns) at two ranges: a=1 and a=1.25 (rows from the top to the bottom, respectively) in one dimension. In each panel, the calculation for the step function (step pot), perturbation correction (pert), and the numerical results (num) are compared.

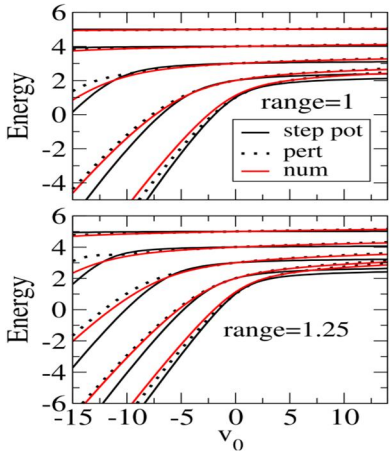

FIG. 5. Comparison of the energy versus v_0 in two dimensions for l = 0, 1, 2, 3, and 4 (from bottom to top) for two ranges: a = 1 and a = 1.25. Even and odd values of l are for bosons and fermions, respectively. Each panel shows results for the step-function (step pot), perturbation correction (pert), and the numerical results (num).

3.2 Eigenvectors

After showing the perturbation treatment results for the eigenvalues, we move now to the illustration of the eigenvectors using the same strategy. In Fig. 6, we compare the ground-state wave functions obtained via three methods (numerical, perturbation, and the step potential). The comparison is illustrated for different values of the strength v_0 and the range a. The three calculations (numerical, perturbation, and the step potential) coincide in the attractive regime (v_0 negative) and for a = 1. In the case of the repulsive regime (v_0 positive) and for the same value of a, the perturbation treatment deteriorates, whereas the results for the step potential are closer to the numerical ones. This is because the neighbouring states are degenerated (fermionization limit), and, consequently, the energy singularity affects the perturbation treatment. We can notice that the situation is worse in 1D. When doing the same calculation for a = 1.5, the perturbation treatment starts to deteriorate even in the attractive regime, while the step-function potential provides a better approximation to the numerically obtained wave functions. The same calculations for the first excited state (Fig. 6) are quite similar, although the perturbation treatment describes the numerical results for the attractive regime and for a = 1 better.

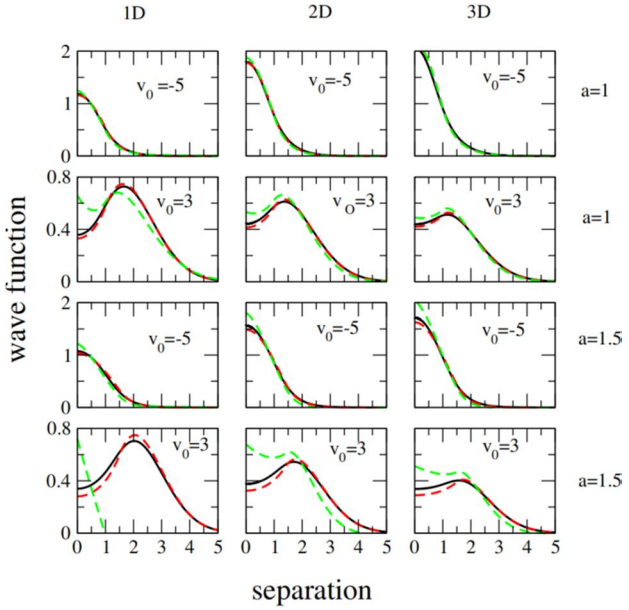

FIG. 6. Ground-state wave function in 1D, 2D, and 3D for the indicated value of the strength v_0 and the range a. Each panel compares the results obtained using the step-function potential (dashed red), the first-order perturbation correction (dashed green), and the full numerical solution (solid black). The three curves are indistinguishable for v_0 = -5 and a = 1 in 3D, though the top of the curves does not appear in order not to change the scale.

To sum up, we can say that the perturbation treatment allowed us to establish a better convergence of the analytical results toward the numerical ones for the energy spectra, whether for the intermediate or important values of the interaction range. However, the perturbation treatment does not yield a noticeable improvement for the eigenvectors of our problem. The results are sensitive to the range of the interaction as well as to the degeneracy of the energy levels occurring in the repulsive regime, especially in 1D. Consequently, the perturbation treatment is failing to establish a more accurate wave function basis to describe few-body problems. We have to notice, however, that, for small ranges, the three calculations are almost indistinguishable across all dimensionalities in the attractive regime, whether for the eigenvectors or the eigenvalues. The perturbation treatment result is even better for the first excited state in the attractive regime. This is setting some considerations for which it is possible to assert that the step potential results and/or ("or" for the case of the first excited level) the corrected ones are giving mainly the exact energies as well as the exact wave functions. Consequently, in the region where these considerations are fulfilled, it is possible to ascertain that we can establish an almost exact analytical wave function basis for describing few-body problems, with higher levels being almost insensitive to the interaction.

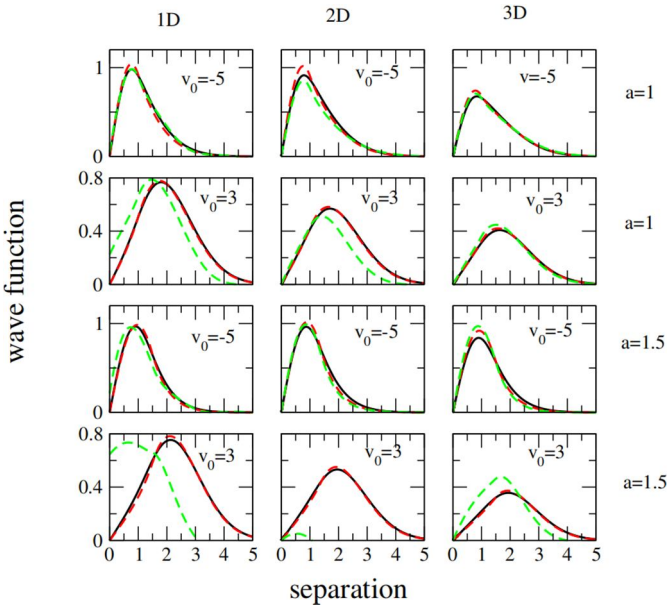

FIG. 7. First excited state wave function in 1D, 2D, and 3D for the indicated value of the strength v_0 and range a. In each panel, the results from the step-function (dashed red), perturbation correction (dashed green), and the numerical results (solid black) are compared.

4. Spatial Correlations

The representation of the energy versus v_0 for different values of the range is frequently used to show the effect of the interaction on the energy spectrum. In order to grasp the dimensionality effect on the spatial correlation, it would be preferable to use an alternative representation: energy spectrum versus the range for different values of v_0. This alternative is presented in Fig. 8 for the case of two dimensions. The advantage of representing energy versus the range over the usually used representation is that it can show the critical range at which we can observe the onset of any change in the different curves. In Fig. 8 and for the attractive regime, one observes that the point of inflection in the energy curves shifts gradually with increasing values of l. It becomes evident that the primary parameter dictating the critical range, where the inflection begins, is the angular quantum number in connection with the strength and the range of the interaction. This is the case even for the first level ($l = 0$), where the onset of the inflection of the curve is not zero but a certain finite value (see discussion in the following section). For the repulsive regime, however, the centrifugal potential and the interaction potential act in the same direction, producing a monotonic increase in energy. The same qualitative behavior is observed in three dimensions, although the energy levels are shifted to higher values due to the increased dimensionality (not shown here for clarity).

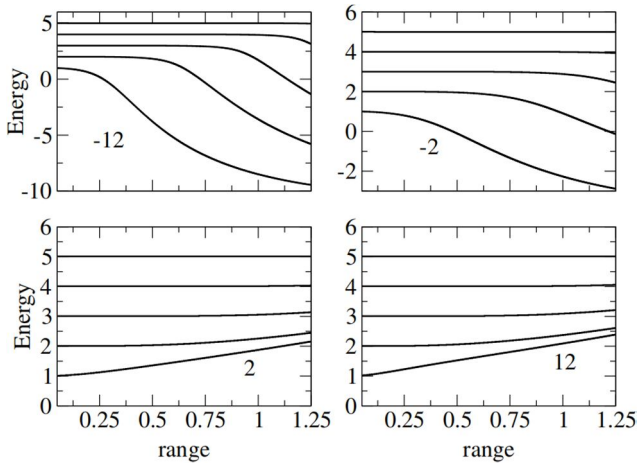

FIG. 8. Energy spectrum for the fundamental relative-radial state (n = 0) versus the range with increasing values of the angular momentum quantum number (l = 0, 1, 2, 3, 4 from bottom to top) in two dimensions. Even values of l are for bosons, and odd ones are for fermions. The numbers on each panel indicate the value of v_0.

The previous results are to be contrasted with the case of 1D in Fig. 9, where the energy is represented versus the range for different values of v_0. One can find that the onset of the inflection is not as gradual for all the levels as previously, when comparing bosonic and fermionic states. Indeed, for the first bosonic state, the inflection starts from zero, whereas for the first fermionic state, a certain critical range has to be reached in order for the inflection to occur. For the higher bosonic and fermionic levels, we can observe an evolution that is not as straight as in the case for the first levels but proceeds via several inflection points and is tightly related to the change of the interaction strength and range. The understanding of the behavior of the first bosonic and fermionic levels is quite straightforward and is due to the additional repulsion resulting from the fermionic statistics. For the repulsive regime, we can observe the same tendency to fermionization, except that in this case, the limits are not flat but continue to increase monotonically with increasing value of the range.

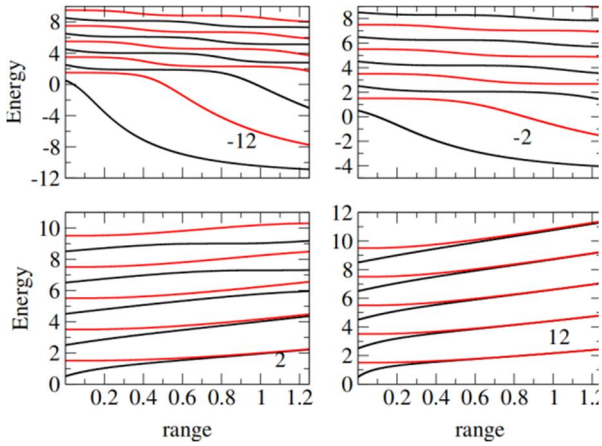

FIG. 9. Energy spectrum in one dimension versus the range with increasing value of n (n = 0, 1,..., 8, from bottom to top) with even values of n for bosons (black) and odd ones for fermions (red). The numbers on each panel indicate the value of v_0 .

We intend to show in this part, by using the results of the previous model (analytical solution for the step-like potential), the impact of the dimensionality on the space correlation of the two particles forming our system. By plotting the energy of the ground state of the relative part of the solution versus the range and for the attractive regime (Fig. 10 (a), v_0 = -5, solid lines), we observe a threshold behavior indicating the onset of binding: the energy becomes increasingly negative, signifying the formation of a bound state. Notably, this critical range, defined as the minimum range at which the attraction begins to significantly lower the energy, depends on the system's dimensionality. Specifically, the critical range is largest in the 3D case, followed by the 2D case, while in 1D, the critical range is effectively zero. The increase

in the case of a repulsive regime (Fig. 10 (a), v_0 = 5, dashed lines) is more straight with no critical range. Interestingly, the energy curves in this case converge to a common limiting value across all three dimensionalities. The different thresholds in the attractive regime are the result of the interplay between the centrifugal repulsion and the attractive interaction. In the case of 1D, the centrifugal potential is absent [Eq. (7)] and, consequently, the critical range is null. For the 3D case, even if we set $l = 0$ for the ground state, we still are left with $l = 1/2$ in 2D, as explained before. Consequently, though the centrifugal potential is equal to zero in this case, still $l_{2D} = 1/2$ appears within the arguments of the confluent hypergeometric solution of the 3D equation [17] and, consequently, this is affecting the solution. Similarly, setting $l = 0$ in 2D will not annihilate the centrifugal potential since in this case we are left with the residual term $\frac{-1/4}{r^2}$ [Eq. (8)]. It is clear from Fig. 10 (a) that the amount of the centrifugal effect is increasing gradually from the 1D case to the 3D case, passing by the 2D case.

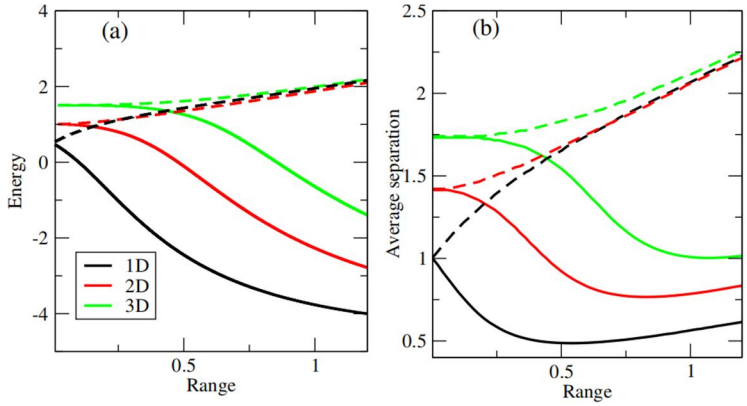

FIG. 10. (a) Comparison of the ground state energy (n = 0 for 1D, and n = 0, l = 0 for 2D and 3D) versus the range of the interaction for the three dimensionalities. (b) Comparison of the average separation between the two particles in the ground state versus the range for the three dimensionalities. Solid curves are for the attractive case (v_0 = -5) and the dashed curves are for the repulsive case (v_0 = 5).

How do these effects impact the spatial or pair correlation? To investigate this point, we plot the average separation between the two particles versus the range of the interaction for the three dimensionalities [Fig. 10 (b)]. The average separation is defined as $\sqrt{\langle x^2 \rangle}$, and the average value is calculated using the normalized total relative function (the radial part of the wave function for 2D and 3D). We plot the average separation versus the range for two different values of v_0 (v_0 = -5 for the attractive regime and v_0 = 5 for the repulsive one). The average separation is evaluated across the full spatial domain, while the interaction range is defined as half the total spatial extent, consistent with earlier sections where the range refers to the distance from the origin to the edge of the step potential (as shown in Fig. 1). This induces a factor of 2 between the two quantities. Let us first notice the similarity between the curves in Figs. 10(a) and 10(b). For the attractive regime in 1D, represented by the black solid curve in Fig. 10 (b), the average separation for a range that is nearly null is 1, consistent with the result for the non-interacting harmonic oscillator ground state. As the range increases, the average separation initially decreases, reaching a minimum, before gradually increasing and saturating. We have to notice here that the decrease occurs smoothly without a critical range. The 2D and 3D cases (Fig. 10(b), red and green solid curves) exhibit a similar trend, but with a noticeable critical range after which the average separation starts to decrease. The critical range and the curve minimum are more important for the 3D case than for the 2D one. These results show that for the 1D case, the average separation starts from a value where interaction has no effect, and when increasing the range, the system immediately feels attraction, and hence it is driven to a closer separation. Afterwards, the saturation of the average separation occurs because of the saturation of the energy for the bonded state [Fig. 10(a)]. This means that no energy is available to drive the system any closer. The same explanation holds for the 2D and 3D cases, except that in these cases, the centrifugal effect enters into play. This results in a starting average separation which is higher and, consequently, a

larger range is needed in order for the system to overcome the centrifugal repulsion and to feel the effect of the attraction. The saturation of the average separation in 2D and 3D is also due to the saturation of the bonding energy. Once the minimum is overcome, the difference in the average separation between the three dimensionalities stays nearly constant. In Fig. 10(b), the repulsive regime ($v_0 = 5$, dashed curves) for the three dimensionalities is also plotted. In this case, the average separation increases gradually for the whole extent of the range. The results for 1D, 2D, and 3D converge to the same limit. This behavior is replicating the behavior of the available energy in the repulsive regime. We also find in this case that the average separation for the three dimensionalities is almost equal to the range of the interaction (bear in mind the factor of 2 between the range and the average separation, as mentioned before). The spatial correlation for the same system is also studied for 1D in Ref. [27] using the two-particle density profile. The results are shown only for the repulsive regime where the inter-particle distance increases gradually with the increase of the range, as confirmed by our calculation. While our method does not resolve the exact localization of particles within the trap, we are able to quantify the average separation on the whole extent of the range for the different dimensionalities and for different regimes in a very simple manner. This approach clearly illustrates the interplay between the interaction strength and the centrifugal potential (which depends on dimensionality) and their combined effect on spatial correlations.

In Fig. 11, we present the same illustration as in Fig. 10 but for the first excited state for the three dimensionalities (n = 0 for 1D, and n = 0, l = 1 for 2D and 3D). The results are quite similar, though it is clear that the critical range at which we have the onset of the inflection in this case is more important, whether for the energy or the average separation. This is expected, as these excited states are fermionic and thus subject to Pauli repulsion. Furthermore, the value of the angular momentum quantum number in 2D and 3D increases the centrifugal potential. As expected, the value of energy for a range that is null as well as the average separation are more important in this case compared to the results for the ground state (Fig. 10). Unfortunately, it is not possible to extend the plot beyond the range of 1.25 (the calculation breaks down because of the singular behavior of the confluent hypergeometric functions beyond the plotted region). However, based on the observed trends, we can expect the same saturation result in the attractive regime.

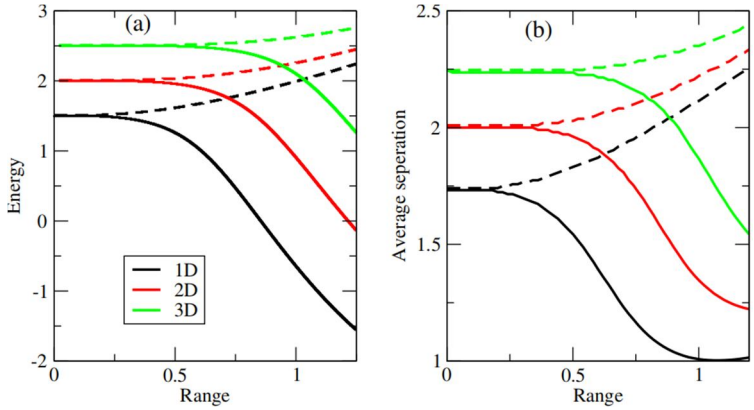

FIG. 11 (a) Comparison of the first excited state energy (n = 1 for 1D; n = 0, l = 1 for 2D and 3D) energy versus the range of the interaction for the three dimensionalities. (b) Comparison of the average separation between the two particles in the first excited state versus the range for the three dimensionalities. Solid curves are for the attractive case (v_0 = -5), and the dashed curves are for the repulsive case (v_0 = 5).

5. **Dynamical Aspects**

There is a growing interest in the study of the non-equilibrium evolution of cold, confined few-particle systems. Recent research in this area has led to intriguing findings that deepen our understanding of the fundamental dynamics governing such systems [30, 32]. In particular, the availability of analytical solutions for certain prototype models has proven to be highly beneficial in exploring key dynamical features. Many of these analytical approaches are based on the assumption of contact interactions, which serve as a reliable approximation in dilute systems [33].

In what follows, we present some preliminary results that can be obtained by using our step-like potential model to describe a system of two confined bosons. The analysis is carried out in a simplified framework, aiming to offer qualitative insight into the potential dynamical behavior of such systems beyond the static properties discussed earlier.

This interaction choice could be a good candidate in the case of Rydberg atom systems. To our best knowledge, no such investigation was carried out before. Only delta-like or Gaussian interactions were studied [33, 34]. The evolution of the system properties with time requires the solution of the time-dependent Schrödinger equation. Our goal is to investigate the evolution of the system under the initial interaction features compared with the change of the behavior of the system under a sudden change of these same features. This is what is known as a quenched interaction. We are elaborating these calculations for the three dimensionalities. To solve the time-dependent Schrödinger equation, we employ the Crank-Nicolson method together with the tridiagonal matrix algorithm, exploiting the built-in programs provided by the LAPACK library [35]. We consider grid sizes of Δt =0.0002 and Δx = 0.04. We take a space of $-30 \leq x \leq 30$. While the time step is fine enough to avoid any distortions during time, the step and the extent of the space are constrained by computational resources. Nevertheless, these are quite satisfactory for the present calculations to reach convergence. The initial wave function from which the evolution of the system starts is considered to be the exact analytical ground state solution already found by resolving the time-independent Schrödinger equation for a step potential interaction. We focus solely on the relative part of the wave function, since the center of motion is not affected by the interaction [Eq. (4)]. This implies that the initial exact ground-state solution we have established by resolving the time-independent Schrödinger equation, is evolves in time, either in the same initial potential or under a suddenly modified potential features at t = 0. In the first situation, we have just a stationary state, and in the second situation, the systems are no longer stationary but start to evolve under the new potential.

5.1 1D Case

In Figs. 12, 13, and 14, we present different quench scenarios, each starting from a different initial point. In Fig. 12, the starting point is v_0 = -5, and the first panel shows the stationary case. This 2D plot illustrates the probability density as a function of both average separation and time. At each time *t*, the probability density is calculated as $f(r)f^*(r)$, where *f(r,t)* is the normalized temporal (either stationnary or quenched) evolution of the wave function *f(r,0),* the properly normalized wave function *f(r,0)* being determined by Eq. (8). This stationary evolution reproduces a well-localized probability distribution with a nearly constant interparticle separation, demonstrating the reliability and internal consistency of our computational implementation. Only very tiny numerical kinks start to develop with time. This is due to the known Crank-Nicolson spurious oscillations that contaminate the wave function at each time iteration without compromising the physical results [36]. From this initial state, we perform different sudden changes on the strength of the potential. We can see that changing v_0 from -5 to -12 confines the probability density to a slightly narrower separation and hence a better localization of the system is reached throughout the whole time interval. Switching the interaction strength from -5 to 0 leads to a breathing mode, characterized by regular oscillations of the average separation between two extreme values. In the case where v_0 is switched from -5 to 12, we can witness a high fragmentation of the density probability with a very poor localization of the system. When we change the starting point (Fig. 13) and set v_0 = 5, the stationary case gives, as expected, two well-localized pics of the probability density. Switching v_0 from 5 to 0 results in a regular pattern with an oscillatory behavior of the separation over time. A sudden change of v_0 from 5 to -12 leads to significant fragmentation of the probability density. Although the resulting pattern remains somewhat regular, there is a clear tendency for the density to shift toward the center, driven by the attractive post-quench interaction. Interestingly, when v_0 is changed from 5 to 12, the system remains nearly in a stationary regime: the separation between the particles is largely preserved, indicating that the increase in repulsion does not significantly push the particles further apart. Let us now investigate the particular case where the starting point is v_0 = 0 (Fig. 14). Here, we have a well-localized pic in the stationary regime. However, setting the

change of v_0 from 0 to -12 gives a variation of the separation between two extreme positions. Changing v_0 from 0 to 12 yields the same result as when starting with v_0 = -5. To summarize these results at the level of the average separation, we present the results for the average separation for the different quench scenarios in Fig. 15. This figure also includes the average separation for the stationary cases (v_0 = -5, 0, and 5, plotted in gray). Additionally, we include the intermediate quenches towards v_0 = 5 or -5. Fig. 15 clearly shows that the already stated oscillatory and fragmented behaviors of the probability density for different scenarios are replicated in the average separation. We can also see that we have only a small perturbation of the average separation around its initial value when we have a transition from attractive to attractive or zero to attractive potential [Figs. 15 (a) and 15(b)] for the transition to the attractive potential. We have this same result when the system is initiated with a repulsive potential, regardless of the nature of the transition operated [Fig. 15 (c)]. However, initiating the system from an attractive potential and operating a transition towards a repulsive potential creates an important average separation as well as an irregular oscillation of its value. It seems that the greater the transition towards an important value of the potential, the longer the system takes to settle into a nearly constant value (note the damping of the oscillations in Fig. 15 (a) for the transition to the repulsive potential).

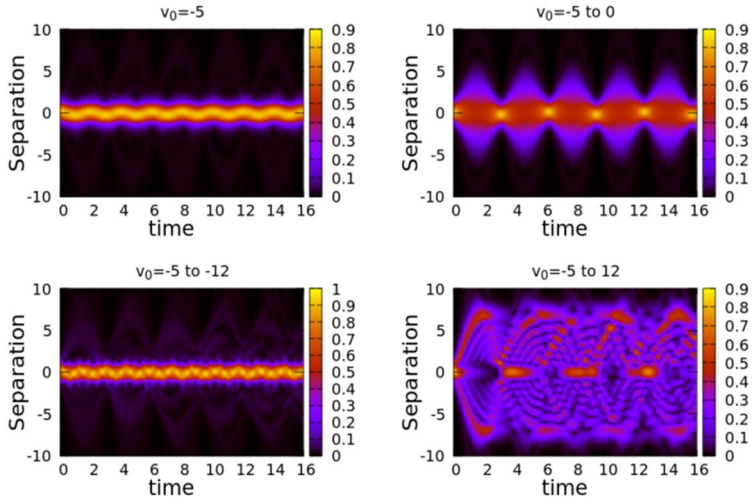

FIG. 12. Time evolution of the probability density for different indicated quench scenarios and one-dimensional fundamental state. The initial state is for v_0 = -5, and the range is fixed to 1.

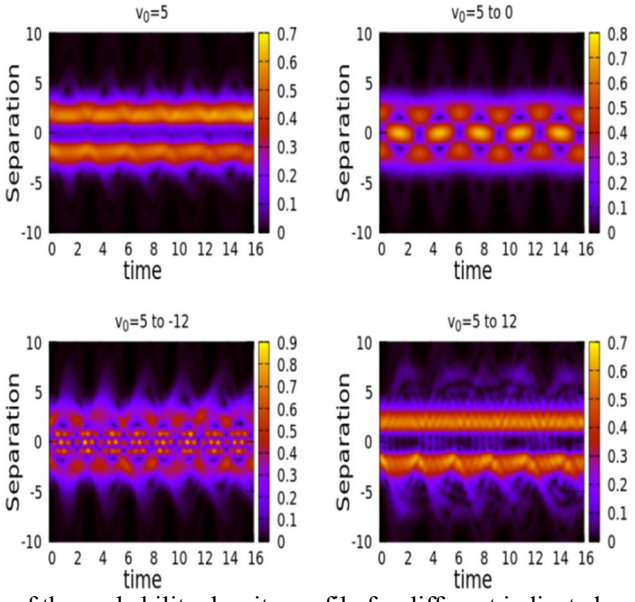

FIG. 13. Time evolution of the probability density profile for different indicated quench scenarios and one-dimensional fundamental state. The initial state is for v_0 = 5, and the range is fixed to 1.

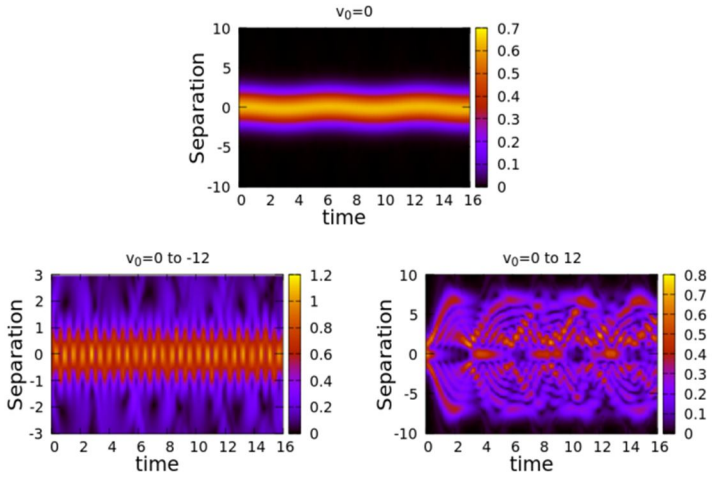

FIG. 14. Time evolution of the probability density profile for different indicated quench scenarios in the one-dimensional fundamental state. The initial state for v_0 is set to 0, and the range is fixed to 1.

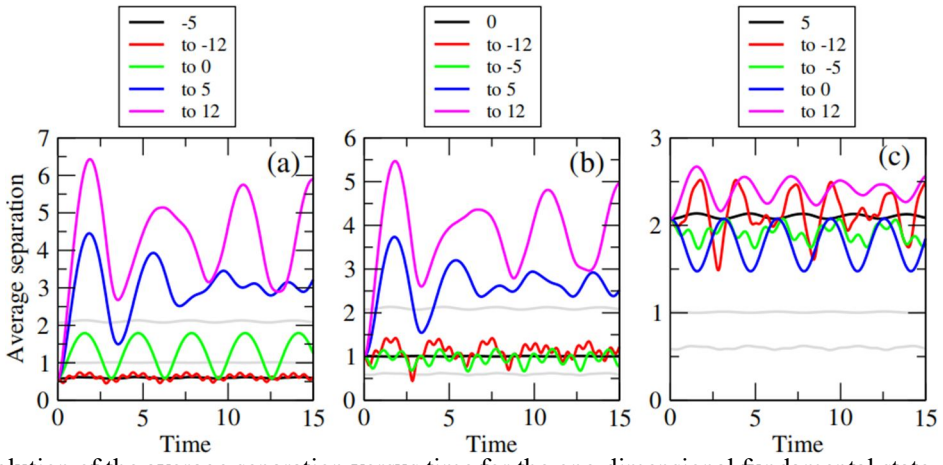

FIG. 15. Evolution of the average separation versus time for the one-dimensional fundamental state. The average separation for the stationary states for each fixed potential is shown in black for the corresponding potential and in gray for the other two potentials in each panel. Different scenarios of sudden changes in the potential strength from the initial value are given in the legend. The range of the interaction is fixed at 1. (a) The initial state is the one for v_0 = -5, (b) the initial state is the one for v_0 = 0, and (c) the initial state is one for v_0 = 5.

5.2. 2D Case

For the 2D case, the probability density at each time t is calculated as $f(r)f^*(r)$, where *f(r,t)* is the normalized temporal (either stationnary or quenched) evolution of the wave function *f(r,0),* the properly normalized wave function *f(r,0)* being determined by Eq. (8). To elaborate the calculation for this part, we are facing the problem of the singularity of the centrifugal potential at r = 0 when we set $l = 0$ in the Eq. (8). In fact, in this case when setting l = 0, we are left with $\frac{-1/4}{r^2}$ for the centrifugal potential. It is not possible to avoid the region where r = 0, as the correlation must be studied in the whole space of the trap. To remedy this situation, the usual numerical solution is to soften the singularity by introducing a small constant α in the denominator [37]. We propose the following transformation:

$$\frac{-1/4}{r^2} \rightarrow \frac{-1/4}{\sqrt{(r^4+\alpha)}} \tag{14}$$

To establish the best choice of the value of α, we must check that it is the smallest value that reproduces the stationary regime. We found that α=0.001 for $v_0 \geq 0$, and α = 0.0000001 for $v_0 < 0$. Using these values for the calculations, we reproduce the same quench scenarios for the 2D case as those shown for 1D in Figs. 16, 17, and 18. Comparing the 1D and 2D results, we notice that qualitatively the behavior is similar, except that the breathing mode seen for the v_0= -5 to 0 has disappeared (Fig. 16). We notice also that the fragmentation for v_0 = -5 to 12 and v_0= 0 to 12 is less pronounced (Figs. 16 and 18). The results for quench scenarios starting from v_0 = 5 are more affected by numerical errors caused by spurious oscillations inherent to the Crank-Nicolson method (Fig. 17). In this scenario, the

fraction of the density probability driven to the center when setting v_0 = 5 to -12 is also less important. We plot the average separation for these different scenarios in Fig. 19. As observed previously, only a quench from an attractive or null potential to a repulsive one is able to noticeably change the spatial correlation between the two particles. However, the transition from an attractive potential to a repulsive one leads obviously to a greater average separation compared to the 1D case. It is important to note here that some of the results could be just numerical artefacts (particularly the disappearance of the breathing mode), and the singularity of the centrifugal potential should be properly dealt with.

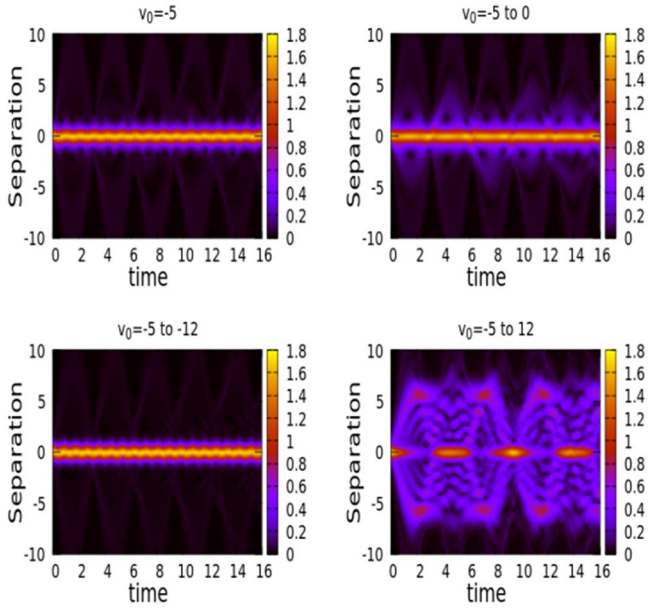

FIG. 16 Time evolution of the probability density for different indicated quench scenarios in the two-dimensional fundamental state. The initial state is v_0 = -5, and the range is fixed at 1.

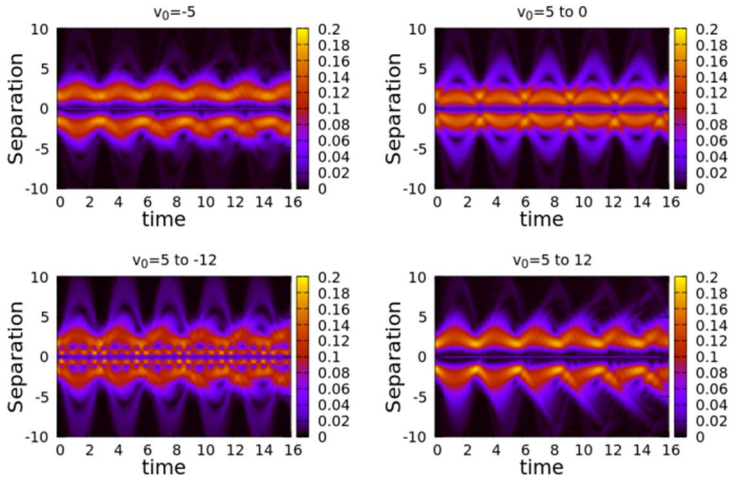

FIG. 17. Time evolution of the probability density profile for different indicated quench scenarios in the two-dimensional fundamental state. The initial state is v_0 = 5, and the range is fixed at 1.

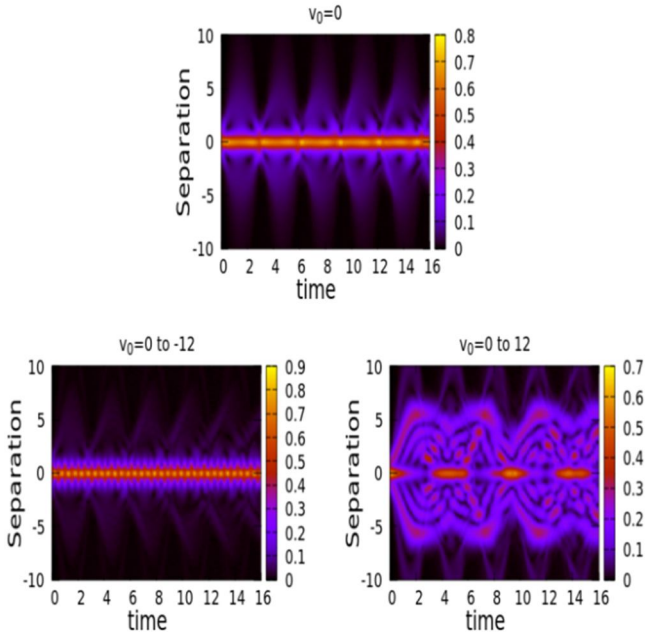

FIG.18. Time evolution of the probability density profile for different indicated quench scenarios in the two-dimensional fundamental state. The initial state is $v_0 = 0$, and the range is fixed at 1.

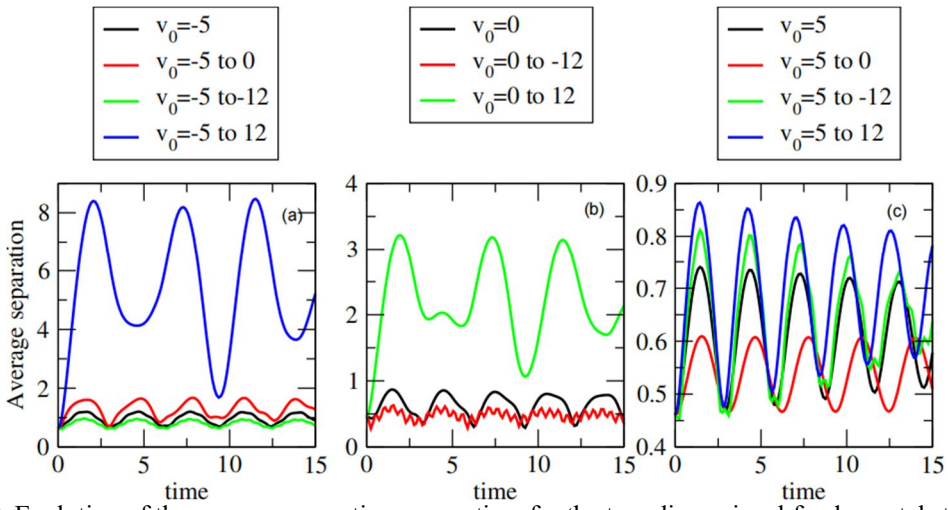

FIG. 19. Evolution of the average separation versus time for the two-dimensional fundamental state. The different scenarios of the sudden change in the potential strength from the initial value are given in the legend. The range of interaction is fixed at 1. (a) The initial state is $v_0 = -5$, (b) the initial state is $v_0 = 0$, and (c) the initial state is $v_0 = 5$.

5.3. 3D Case

For the 3D case, the probability density at each time t is calculated as $f(r)f^*(r)$, where *f(r,t)* is the normalized temporal (either stationary or quenched) evolution of the wave function *f(r,0)*. The properly normalized wave function *f(r,0)* is determined by Eq. (9). As we have explained before, in the 3D case setting $l_{3D} = 0$ for the fundamental state means $l_{2D} = 1/2$ [see Eq. (10)]. This value of the angular quantum number appears in the argument of the confluent hypergeometric function, influencing the results even if apparently the centrifugal potential is reduced to zero. For the sake of brevity, we present only the average separation for the different quench scenarios in the 3D case (Fig. 20). Qualitatively, the results are the same as before. However, the average separation is notably larger when the system undergoes a transition from an attractive to a repulsive potential [Fig. 20 (a)]. Moreover, transitions from a repulsive potential show less sensitivity to perturbations compared to the other dimensionalities [Fig. 20 (c)].

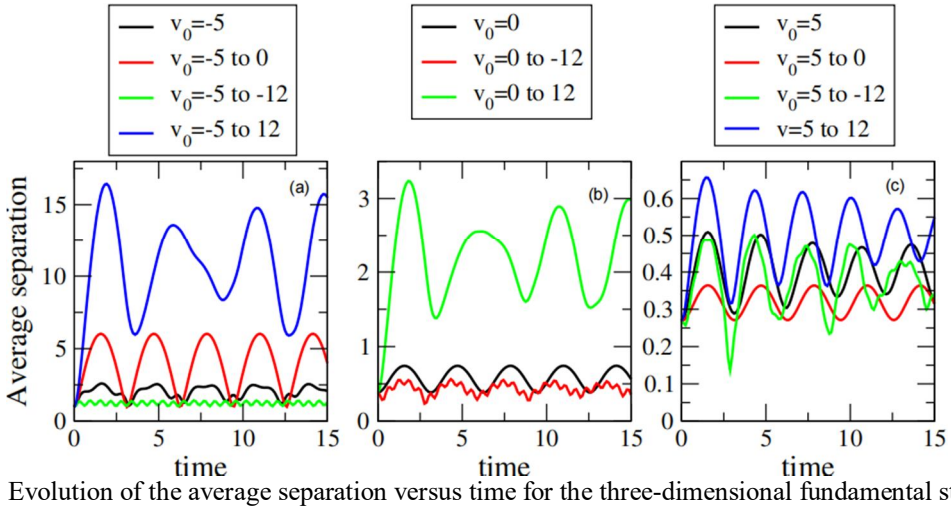

FIG. 20. Evolution of the average separation versus time for the three-dimensional fundamental state. The different scenarios of sudden changes in the potential strength from the initial value are given in the legend. The range of interaction is fixed at 1. (a) The initial state is v_0 = -5, (b) the initial state is v_0 = 0, and (c) the initial state is v_0 = 5.

6. Conclusion

The aim of this study is to highlight the features that arise in different aspects of a system of two Rydberg atoms confined in a harmonic trap under different dimensionalities. To conduct the study, we use the exact solution provided by the Schrödinger equation with a step-like potential. To prove the adequacy of this model for describing the targeted Rydberg interactions, we developed a perturbation treatment of the proposed model. The results offer a more accurate description of the energy spectra. The results for eigenvectors are less satisfactory, fundamentally because of the energy degeneracy between neighboring levels, which causes the mathematical formulation to become singular. Far from the region where this degeneracy occurs, it is possible to establish acceptable results that could be fairly used as a wave function basis for few-body systems. Being more confident about the used model, we move in the second part to the characterization of the spatial correlation of the studied system. The results shed light on the role played by the interrelation between the interaction features and the centrifugal potential arising from the considered dimensionality, and how this interplay affects spatial correlations. In the attractive regime, a complex behavior emerges because the interaction and centrifugal repulsion act antagonistically. In contrast, in the repulsive regime, where interaction and centrifugal repulsion act in the same direction, the spatial correlation is primarily dictated by the interaction features. For both regimes, the results also demonstrate the impact of the energy available to the state, which clearly influences the overall trend of spatial correlation. In the final part, we investigate the effect of dimensionality on the temporal evolution of the system under different quench scenarios. Here, we also employ the exact solution for the step-like interaction. This specific interaction must be contrasted with delta-like and Gaussian interactions, as the step-like interaction is spatially extended with a constant strength over the considered range, unlike the localized delta or Gaussian potentials. Our preliminary results illustrate how the density profile evolves and reveal how the quench scenario affects the probability density distribution and, consequently, the spatial correlation of the system.

In this study, the quench is applied solely to the interaction strength, but it can be easily extended to the interaction range as well. Gathering extensive data on these dynamical aspects while distinguishing numerical artifacts could provide important insights into both theoretical and technological aspects of cold few-particle systems. A deeper investigation along these lines could shed more light on fundamental aspects related to strongly correlated systems and may also offer experimental clues on how to monitor system correlations.

References

[1] Blume, D., Rep. Prog. Phys., 75 (2012) 046401.

[2] Abraham, J.W. and Bonitz, M., Contrib. Plasma Phys., 54 (2014) 27.

[3] Turbiner, A.V., Phys. Rep., 642 (2016) 1.

[4] Morales, J., Garcia-Martinez, J., Garcia-Ravelo, J., and Pena, J.J., J. Appl. Math. Phys., 3 (2015) 454.

[5] Gao, B., Phys. Rev. A, 58 (1998) 1728.

[6] Gao, B., Phys. Rev. A, 59 (1999) 2778.

[7] Ginocchio, J.N., Ann. Phys., 152 (1984) 203.

[8] Blaizot, J-P. and Ripka, G., "Quantum Theory of Finite Systems", 1st Ed., (MIT Press, Massachusetts, 1985).

[9] Pitaevskii, L. and Stringari, S., "Bose-Einstein condensation", 1st Ed., (Clarendon Press, Oxford, 2003).

[10] Kościk, P., Kuroś, A., Pieprzycki, A., and Sowiński, T., Sci. Rep., 11 (2021) 13168.

[11] Busch, T., Englert, B-G., Rzazewski, K., and Wilkens, M., Found. Phys., 28 (1998) 549.

[12] Wei, B-B., Int. J. Mod. Phys. B, 23 (2009) 3709.

[13] Doganov, R.A., Klaiman, S., Alon, O.E., Streltsov, A.I., and Cederbaum, L.S., Phys. Rev. A, 87 (2013) 033631.

[14] Mujal, P., Polls, A., and Julia-Diaz, B., Condens. Matter, 3 (2018) 9.

[15] Ołdziejewski, R., Górecki, W., and Rzaźewski, K., Europh. Lett., 114 (2016) 4.

[16] Lim, J., Lee, H-G., and Ahn, J., J. Korean Phys. Soc., 63 (2013) 867.

[17] Kościk, P. and Sowiński, T., Sci. Rep., 8 (2019) 12018.

[18] Zinner, P.N.T., EPJ Web Conf., 113 (2016) 01002.

[19] Islam, R. et al., Science, 340 (2013) 583.

[20] Görlitz, A. et al., Phys. Rev. Lett., 87 (2001) 130402.

[21] Grar, N. and Chia, L., J. Phys. Chem. Res., 1 (2022) 7.

[22] Gallagher, T.F., Rep. Prog. Phys., 51 (1988) 143.

[23] Dalibard, J., "Les Interactions Entre Atomes Dans Les Gaz Quantiques", (College de France, lecture notes, 2020) [in French].

[24] Mathews, Jr.W.N., Esrick, M.A., Teoh, Z., and Freerick, J.K., "A Physicist's Guide to the Solution of Kummer's Equation and Confluent Hypergeometric Functions", (arxiv, 2021).

[25] Abramowitz, M. and Stegan, I., "Handbook of Mathematical Functions with Formulas, Graphs, and Mathematical Tables", 10th Ed., (U.S. Government Printing Office, Washington, 1964).

[26] Digital Library of Mathematical Functions, (2021), http://dlmf.nist.gov.

[27] Kościk, P. and Sowiński, T., Sci. Rep., 8 (2018) 48.

[28] Girardeau, M., J. Math. Phys., 1 (1960) 516.

[29] Okopińska, A. and Kościk, P., Few-Body Syst., 45 (2009) 223.

[30] Dobrzyniecki, J. and Sowiński, T., Phys. Rev. A, 103 (2021) 013304.

[31] Giannozzi, P., Ercolessi, F., and Gironcoli, S.D., "Numerical Methods in Quantum Mechanic", (Lecture notes, 2021).

[32] Kehrberger, L.M.A., Bolsinger, V.J., and Schmelcher, P., Phys. Rev. A, 2018 (2018) 01360697.

[33] Budewig, L., Mistakidis, S.I., and Schmelcher, P., Mol. Phys., 117 (2019) 2043.

[34] Ishmukhamedov, I.S., Phys. E, 142 (2022) 115228.

[35] Koonin, S.E. and Meredith, D.C., "Computational Physics: Fortran Version", 1st Ed., (CRC Press, 1990).

[36] Neto, A.B., Mansur, W.J., and Ferreira, W.G., Sci. Rep., 12 (2022) 18887.

[37] Loudon, R., Am. J. Phys., 27 (1959) 649.